Noname manuscript No.
(will be inserted by the editor)

Polarization observables in double-charged-pion photo-production with circularly-polarized photons off transversely-polarized protons

L. A. Net · S. Strauch · (For the CLAS Collaboration)

Received: date / Accepted: date

Abstract Double-pion photo-production represents one of the strongest contributions to the photonucleon total cross-section at high energies, and thus it plays an important role in probing the nucleon resonance spectrum. The polarization observables are useful because of the additional sensitivity they provide in unraveling the reaction dynamics, and so the goal of this study is to extract the specific polarization observables $I^{\odot}$, P_x, P_y, $P_x^{\odot}$, $P_y^{\odot}$, for the $\gamma p \to p\pi^+\pi^-$ reaction. The data were taken as a part of the CLAS g9b (FROST) experiment at Jefferson Laboratory, which used a transversely-polarized target and a circularly-polarized photon beam with energies up to 3 GeV. The data will help deepen the current knowledge of resonance photocouplings and hadronic decays and possibly assist in identifying new baryon resonances via partial-wave analyses and in this way will contribute to a more comprehensive understanding of the strong interaction.

1 Introduction

Understanding the complex interaction between quarks and gluons inside protons and neutrons remain one of the most significant challenges of physics today since perturbative QCD calculations fail to provide solutions in this low-energy regime and thus alternative pathways are needed to explore the complex structure and interactions of baryons. Many theoretical models including lattice-QCD calculations predict a rich nucleon spectrum with more excited states than have been observed experimentally [1]. An ongoing experimental effort is underway to look for these missing baryons, and the FROST experiment, as part of Jefferson Lab's N^* program, is measuring new polarization observables in photoproduction experiments

This work is supported in parts by NSF PHY-1505615.

L. A. Net
University of South Carolina, Columbia, SC, USA

S. Strauch
University of South Carolina, Columbia, SC, USA

off polarized protons. The present work tries to address the "missing resonance" problem by analyzing the $\boldsymbol{\gamma p} \to p\pi^+\pi^-$ reaction channel in order to extract the polarization observables $I^{\odot}$, P_x, P_y, $P_x^{\odot}$, and $P_y^{\odot}$ specific to the interaction of a circularly-polarized photon beam with a transversely-polarized target. Figure 1 shows a schematic view of the reaction in the center-of-mass frame along with angle definitions. The polarized cross-section for this reaction is [2]:

$$\frac{d\sigma}{d\Omega} = \frac{d\sigma_0}{d\Omega}\left[1 + P_x \Lambda \cos\alpha + P_y \Lambda \sin\alpha + \delta_{\odot}\left(I^{\odot} + P_x^{\odot}\Lambda\cos\alpha + P_y^{\odot}\Lambda\sin\alpha\right)\right], \tag{1}$$

where σ_0 is the unpolarized cross-section, α is the angle between the target polarization and the reaction plane, Λ is the degree of the target polarization, $\delta_{\odot}$ the degree of the photon-beam polarization, and $I^{\odot}$, P_x, P_y, $P_x^{\odot}$, $P_y^{\odot}$ are the observables to be extracted in this analysis. Relevant information about the resonances can then be obtained through general amplitude analyses or in comparison with specific reaction-model predictions.

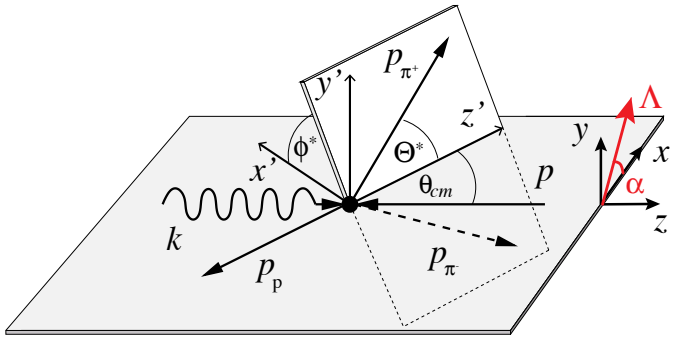

Fig. 1 Schematic sketch of the $\gamma p \to \pi^+\pi^- p$ reaction in the γp center of mass, where k and p are the momenta of the photon and of the target proton, and p_p, p_{π^+} and p_{π^-} are the momenta of the recoiling proton, π^+ and π^-, respectively. The red arrow Λ indicates the target-polarization direction, transverse to the beam. Figure adapted from [3].

2 Experiment

The FROST g9b experiment ran in 2010 at Jefferson Lab in Hall B. A longitudinally-polarized electron beam from the CEBAF accelerator with an energy of E_e = 3081.73 MeV hit a thin bremsstrahlung target to produce a circularly-polarized photon beam that is energy-tagged in the Hall-B photon tagger [4]. The energy of the tagged photon beam ranged between 20% and 95% of the energy of the incident electron beam covering a center-of-mass energy range from W = 1450 MeV to 2550 MeV in the γp reaction. The degree of photon-beam polarization $\delta_{\odot}$ [5],

$$\delta_{\odot} = P_e \frac{4x - x^2}{4 - 4x + 3x^2}, \tag{2}$$

is proportional to the electron-beam polarization P_e and a function of the ratio of the photon and electron energies, $x = E_\gamma/E_0$. The average electron-beam polarization was $\bar{P}_e = 87.04 \pm 0.70$, and the photon-beam helicity was flipped between $+1$ and -1 at a frequency of up to 1 kHz.

The photon beam was collimated before impinging on a 5-cm long frozen-spin butanol target [6] in the center of the CEBAF Large Acceptance Spectrometer (CLAS). The free protons of the butanol target were polarized through dynamic nuclear polarization. To help maintain the polarization, the target temperature was reduced to 30 mK, and a holding magnetic field of 0.5 T was applied. Reactions off unpolarized nuclei other than the polarized protons lead to a background that was studied with additional carbon and polyethylene targets downstream of the butanol target. The proton-target polarization ranged on average from 75% to 86%, and its direction was regularly reversed to minimize systematic uncertainties from instrumental asymmetries.

The CLAS spectrometer [7] was used for detecting the charged particles in the final-state.

3 Data Analysis

The particles of interest, π^+, π^-, and p, were identified by their charge and by their mass through time-of-flight measurements. Cuts were placed on the difference between the measured speed β and the calculated speed of each particle,

$$\Delta\beta = \beta - \frac{p}{\sqrt{p^2 + m^2c^2}}, \tag{3}$$

where p is the momentum and m is the mass of the particle.

The $\gamma p \to \pi^+\pi^- p$ reaction was identified in this kinematically complete experiment by the missing-mass technique, requiring either the detection of all three final-state particles or the detection of two out of the three particles in the CLAS detector (four distinct event topologies) in addition to a time-coincidence of the tagged photon and the hadrons at the reaction vertex. The detector acceptances for events from these four distinct topologies are different. The analysis combines data from all topologies to maximize the acceptance. Still, the comparison of the experimental results with model predictions needs to take into account the finite CLAS acceptance.

based on events from different topologies do therefore not have to be consistent.

Data from the butanol target include the signal events of interest from the polarized γp reaction. The sample, however, includes also substantial background from reactions on bound nuclei. The method to separate signal events from background events was a probabilistic weighting method [8]. The main idea of this method is to determine the probability for a given event i to be a signal event, Q_i, or a background event, $1 - Q_i$. The data were pre-binned in 50-MeV wide center-of-mass energy bins. For each event a (called seed event), 5 000 kinematically nearest neighbors were selected within the same event topology. The distance measure between two events a and b that indicates how close two events are in the space defined by the five kinematic variables Γ_k is

$$D^2_{a,b} = \sum_{k=1}^{5} \left(\frac{\Gamma_k^a - \Gamma_k^b}{\Delta_k} \right)^2 . \tag{4}$$

Three angles $\cos\theta^*$, $\cos\theta_{CM}$, ϕ^*, as well as the invariant masses $m_{p\pi^+}$ and $m_{\pi^+\pi^-}$ were chosen for the kinematic variables Γ_k. Δ_k is a norm for each variable. Nearest neighbors were considered from both, the carbon and butanol targets. Events from the carbon target helped fitting the background in the butanol-event sample. Figure 2 shows one example of butanol and carbon missing-mass-squared distributions of the 5 000 nearest neighbors of one seed event for which the p and π^+ were detected. A simultaneous fit of each distribution was performed with a polynomial function for the carbon-event distribution and the scaled polynomial plus a Gaussian distribution for the butanol-target background and signal. The fit result allows to estimate the Q-value of the seed event.

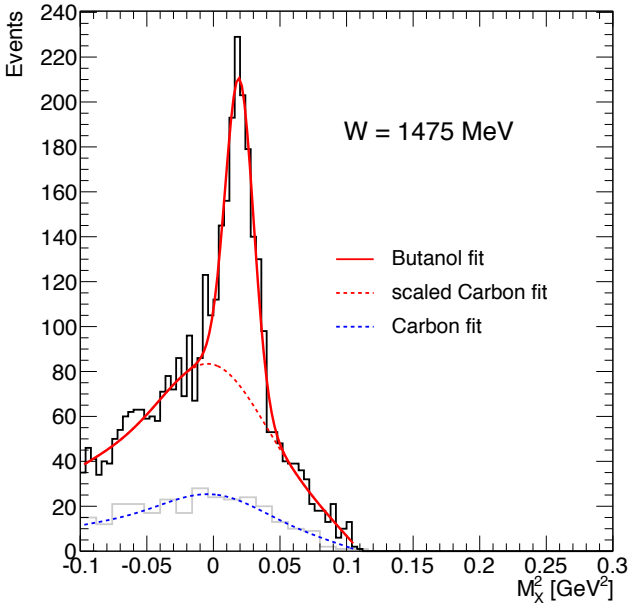

Fig. 2 Missing-mass-squared distribution of 5 000 nearest neighbors for a seed event with undetected π^- and $M_X^2 = 0.026$ GeV^2. The solid red curve shows the fit to the butanol data, the dotted blue curve shows the polynomial fit to the carbon distribution and the dotted red curve depicts that polynomial scaled to fit the butanol distribution. The Q-value for the seed event in this example is $Q = 0.63$.

The observables $I^\odot$, P_x, P_y, $P_x^\odot$, and $P_y^\odot$ were obtained through weighted sums from the Q-values of each event, the per-event target-polarization direction α_i and beam helicity H_i, and the average degrees of beam and target polarizations. The detailed analysis also took into account the relative luminosity in the various run groups and their individual polarization-degree averages. However, the simplified

expressions,

$$\bar{I}^{\odot} = \frac{\sum_i H_i}{\delta_{\odot} \sum_i Q_i} \tag{5}$$

$$\bar{P}_x = \frac{1}{\bar{A}} \frac{\sum_i \cos\alpha_i}{\sum_i Q_i \cos^2\alpha_i}, \tag{6}$$

$$\bar{P}_y = \frac{1}{\bar{A}} \frac{\sum_i \sin\alpha_i}{\sum_i Q_i \sin^2\alpha_i}, \tag{7}$$

$$\bar{P}_x^{\odot} = \frac{1}{\bar{A}} \frac{1}{\bar{\delta}_{\odot}} \frac{\sum_i H_i \cos\alpha_i}{\sum_i Q_i \cos^2\alpha_i}, \text{ and} \tag{8}$$

$$\bar{P}_y^{\odot} = \frac{1}{\bar{A}} \frac{1}{\bar{\delta}_{\odot}} \frac{\sum_i H_i \sin\alpha_i}{\sum_i Q_i \sin^2\alpha_i}, \tag{9}$$

illustrate the method. The most significant contributions to the systematic uncertainties in the polarization observables come from the knowledge of the beam and target polarizations and the estimate of the event background. The regular reversal of the target-polarization orientation cancels most of the instrumental asymmetries caused by, e.g., detector inefficiencies. Temporal changes of the detector efficiency, however, need to be addressed separately.

4 Results

An overview of preliminary results for the five polarization observables is shown in Fig. 3. The observables are given as functions of the π^+ azimuthal angle about the axis that is defined by the recoiling-proton momentum, $-p_p$. The results for the polarization observable $I^{\odot}$ were compared to the previous published results for the experiment g1c [3]; see Fig. 4 for one example. Although different types of targets were used by the g1c (liquid hydrogen target) and g9b experiments (butanol target), the two experimental results agree. The other results are first-time measurements for the observables P_x, P_y, $P_x^{\odot}$, and $P_y^{\odot}$. The data exhibit the symmetry properties that are expected from parity conservation. Observables $I^{\odot}$, P_x, and $P_y^{\odot}$ are odd, and observables $P_x^{\odot}$ and P_y are even functions. The former three observables do not exist in single-pion photoproduction, the latter two correspond to the F and T observables. The data in Fig. 3 are compared with fits of low-order polynomials in $\sin\phi$ and $\cos\phi$ to highlight the symmetry properties. The relative systematic uncertainties of the polarization observables are approximately 5% to 6%, with the most substantial contributions from uncertainties of the target and photon-beam polarizations.

A more differential look at the data is given in Fig. 5. By way of example, the preliminary results for ϕ^* angular distributions of the double-polarization observable $P_y^{\odot}$ are shown for seven non-equidistant bins of $\cos\Theta^*$ and center-of-mass energies $W = 1550$ MeV to 1650 MeV. The data are compared with results from an effective Lagrangian model by A. Fix [9]. The model includes resonance and Born contributions. It gives a satisfactory description of the total cross sections of two-pion production on the proton. However, the shape and strength of the asymmetries of polarization observables depend strongly on the internal mechanisms and interferences among different contributions to the process as was shown for

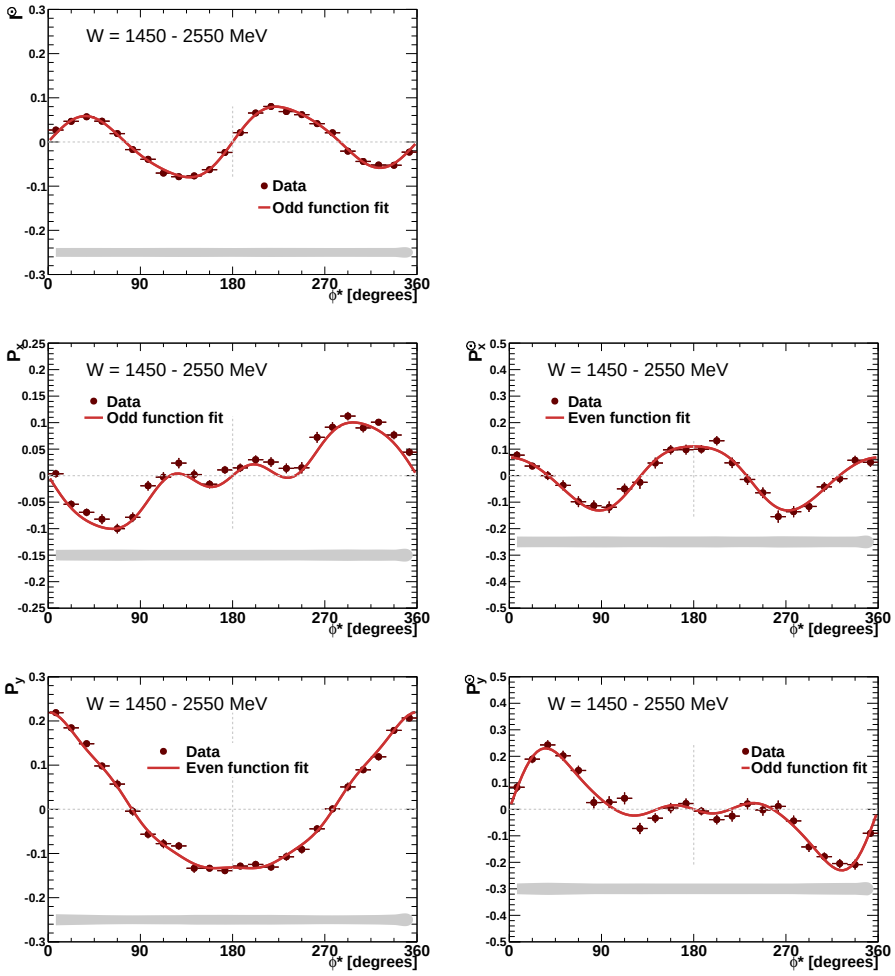

Fig. 3 Preliminary polarization observables $I^{\odot}$, P_x, P_y, $P_x^{\odot}$, and $P_y^{\odot}$ as function of the π^+ azimuthal angle, integrated over the CLAS acceptance and all kinematic variables. The solid curves show low-order even and odd Fourier polynomials. The grey bands indicate preliminary estimates of the size of systematic uncertainties.

the case of the beam helicity asymmetry $I^{\odot}$ [10]. Figure 5 shows limited to fair agreement between the preliminary data and the calculations, indicating that the data can help improve this and other models.

In summary, preliminary results for polarization observables $I^{\odot}$, P_x, P_y, $P_x^{\odot}$, and $P_y^{\odot}$, for the $\gamma p \to p\pi^+\pi^-$ reaction have been extracted from data of the CLAS FROST experiment. The data pose strong constraints on model calculations and provide new information that may lead to a better understanding of the nucleon resonance spectrum and the non-resonant background in the reaction.

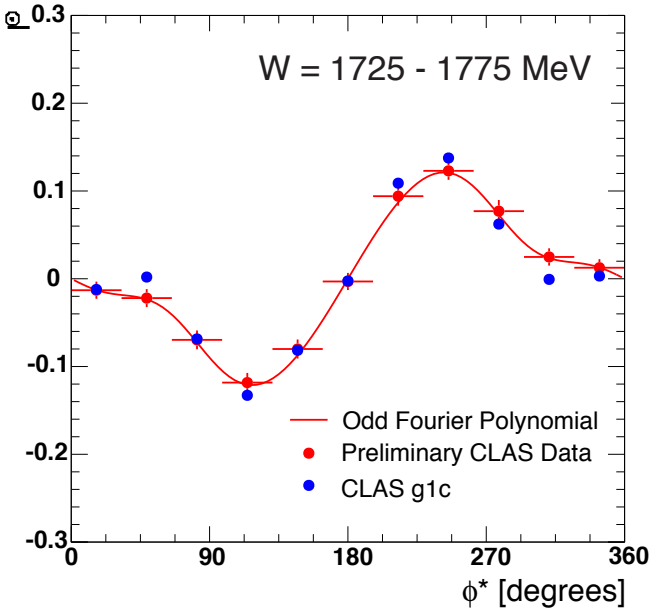

Fig. 4 Comparison of preliminary estimates for the helicity asymetry $I^{\odot}$ from this work (red pionts) with previous results from CLAS g1c [3] (blue points). The data are for the center-of-mass energy range $W = 1725$ MeV to 1775 MeV and integrated over the full CLAS acceptance. Only statistical uncertainties are shown. The two data sets are in resonable agreement.

References

1. V. Credé, W. Roberts, Rept. Prog. Phys. **76**, 076301 (2013). DOI 10.1088/0034-4885/76/7/076301
2. W. Roberts, T. Oed, Phys. Rev. **C71**, 055201 (2005). DOI 10.1103/PhysRevC.71.055201
3. S. Strauch, et al., Phys. Rev. Lett. **95**, 162003 (2005). DOI 10.1103/PhysRevLett.95.162003
4. D.I. Sober, et al., Nucl. Instrum. Meth. **A440**, 263 (2000). DOI 10.1016/S0168-9002(99)00784-6
5. H. Olsen, L.C. Maximon, Phys. Rev. **114**, 887 (1959). DOI 10.1103/PhysRev.114.887
6. C.D. Keith, J. Brock, C. Carlin, S.A. Comer, D. Kashy, J. McAndrew, D.G. Meekins, E. Pasyuk, J.J. Pierce, M.L. Seely, Nucl. Instrum. Meth. **A684**, 27 (2012). DOI 10.1016/j.nima.2012.04.067
7. B.A. Mecking, et al., Nucl. Instrum. Meth. **A503**, 513 (2003). DOI 10.1016/S0168-9002(03)01001-5
8. M. Williams, M. Bellis, C.A. Meyer, JINST **4**, P10003 (2009). DOI 10.1088/1748-0221/4/10/P10003
9. A. Fix, H. Arenhövel, Eur. Phys. J. **A25**, 115 (2005). DOI 10.1140/epja/i2005-10067-5
10. L. Roca, Nucl. Phys. **A748**, 192 (2005). DOI 10.1016/j.nuclphysa.2004.10.028

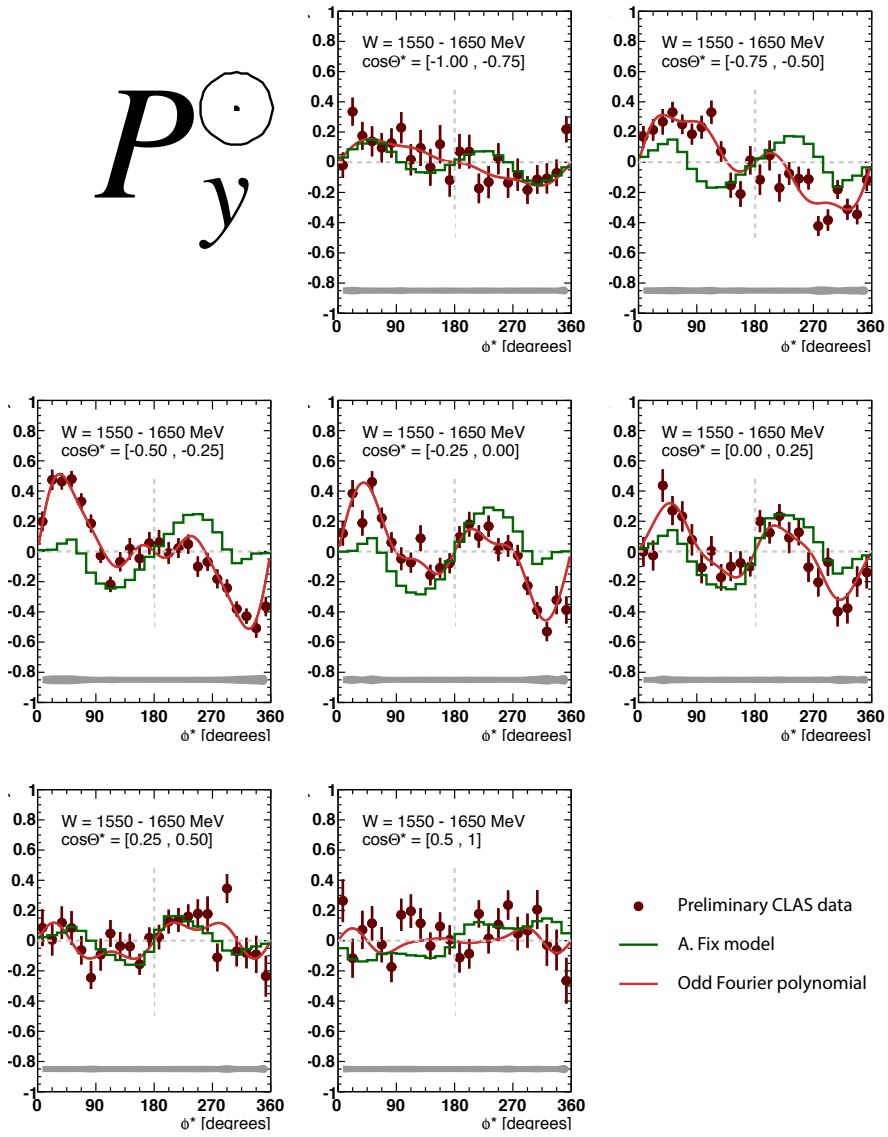

Fig. 5 Examples of preliminary angular distributions of the polarization observable $P_y^{\odot}$ from CLAS in seven bins of $\cos\Theta^*$ for the energy range $W = 1550$ MeV to 1650 MeV. The solid red curves show odd low-order Fourier polynomials to guide the eye. The solid green histograms are CLAS-acceptance corrected results of model calculations from A. Fix [9].